THE UNIVERSITY *of* EDINBURGH
School of Physics
and Astronomy

Modelling of Compton scattering within the Fast ATLAS Track Simulation

MPhys Project Report

Alexis Papandreou

Submitted for the 20pt MPhys Project course PHYS11050
May 5, 2025

CERN-THESIS-2025-040
/ /2025

Abstract

The Fast ATLAS Tracking Simulation (FATRAS) is a computationally efficient tool being developed to simulate the particle interactions within the inner detector of the ATLAS experiment. The development of accurate fast-simulation tools is essential to handling the increased event rates of the upcoming High-Luminosity Large Hadron Collider. This project addresses the lack of Compton scattering modelling in FATRAS by implementing the Klein-Nishina (KN) differential cross-section and developing a parametrised model for the KN total cross-section. The implemented model of Compton scattering demonstrates strong agreement when compared to benchmark Geant4 simulations. Further, a promising parametrisation of the integrated KN cross-section is presented, offering an efficient alternative to direct integration. Future work involves benchmarking the computational performance of the differential cross-section implementation and integrating the total cross-section model into FATRAS.

Supervisor: Dr. Dominik Duda

Contents

1 Introduction

The mission of High Energy Physics (HEP) as a whole is to probe the universe at it most fundamental level, in an attempt to understand the elementary constituents of matter and their interactions.

To interpret the data generated by the incredible machines available to the particle physics community such as ATLAS [1, 2] at the Large Hadron Collider (LHC), detailed simulations are required. These simulations provide a system with which a signal readout on a detector can be reconstructed into a particle trajectory and interaction. As a result, our best theoretical models can be tested against experiment.

The current workhorse of ATLAS simulation is Geant4 [3, 4], a toolkit capable of precise physics modelling. However, as the LHC prepares for the High Luminosity LHC (HL-LHC) [5, 6] era, more computationally efficient simulation methods need to be deployed to handle the vast increase in data. The aim is to maintain a 1:1 ratio of experimental and simulated events despite the increase in luminosity.

Various fast simulation tools are being developed to address these needs, with each tool corresponding to different sections of the ATLAS detector. The Fast ATLAS Tracking Simulation (FATRAS) is a fast simulation engine of the inner detector [7, 8, 9, 10, 11, 12], which aims to strike the balance between accuracy and speed, ensuring enough events can be generated to keep up with the upcoming demands of HL-LHC.

A key part of producing accurate physics results is the accurate modelling of photon interactions with the detector material. Photons can undergo various processes, most notably pair production, Compton scattering and the photoelectric effect. Before the work presented in this report, only pair production was modelled in FATRAS, omitting Compton scattering, the scattering of photons off electrons. With a need to improve the physics performance of FATRAS, the implementation of Compton scattering is a well motivated. The methodology and outcomes of this implementation are reported. Ideally, a fast alternative to the full theoretical treatment of Compton scattering is also developed for use in FATRAS.

The report is organised as follows: Section 2 re-poses the computational challenges presented by the HL-LHC era to ATLAS and establishes some terminology used in relativistic kinematics, along with the theoretical background of the Compton scattering process. This leads into Section 3 (ATLAS Simulation basics), which provides more detail of the simulation frameworks used in ATLAS and how they can be utilised to generate the data presented later in the report. Section 4 (Methods) details the developed methodology for implementing Compton scattering into FATRAS. The priority is the implementation of the differential cross-section, which dictates what happens once Compton scattering is called, however at the end of the section, a proposed parametrisation of the total cross-section is presented. The outcomes of both of these endeavours are presented in Section 5 (Results and Discussion), after an exploration of the theoretical results expected to be achieved. Finally, Section 6 (Conclusion and Future Outlook) will reflect on the success and limitations of the proposed implementations, leaving clear ideas for how to finalise the integration of Compton scattering into FATRAS.

2 Background

This section starts with a short introduction to the ATLAS collaboration, making a case for its significant computational demand and how this will be enhanced by the upcoming upgrades to the Large Hadron Collider (LHC). This is followed by some of the foundational physics principles that govern the photon interactions implemented and analysed later in this report.

2.1 ATLAS at the LHC

The LHC at CERN is one of the largest scientific instruments on the planet, with a global community of thousands of scientists pushing the frontiers of fundamental particle physics. ATLAS is one of two general-purpose detectors on the ring and investigates a broad range of physics. These investigations are facilitated by six sub-detectors working together to identify the characteristics of the collision debris flying away from the collision point of the particle beams.

In order to form tests of the Standard Model or different new-physics models, detailed simulation of the detector response to these high energy collisions is necessary.

2.2 High-Luminosity LHC

To sustain the discovery potential of the LHC, a large upgrade to the instantaneous luminosity (rate of collisions) and the integrated luminosity (total collisions) of the machine is needed. Run 4, also the first High-Luminosity LHC (HL-LHC) run is planned to begin in June 2030 [6], and thus begins a new era of unprecedented data rates; enabling more detailed studies of rare processes and permitting better statistical precision on current measurements.

The substantial increase in collision rates evidently require more computational resources, but a 1:1 increase in computational capacity is untenable by the collaboration due to resource constraints, meaning a more efficient computing model is necessary for the success of HL-LHC. To proceed, it would be useful to introduce the role of Monte-Carlo (MC) methods in High Energy Physics.

2.3 Monte Carlo methods

MC methods have become indispensable in HEP for simulating the complex, probabilistic processes that occur during particle interactions and decays. These methods use random sampling to generate ensembles of events that can emulate the statistical nature of physics processes. In HEP, MC methods are used to:

- Model the generation of particles in high-energy collisions.
- Simulate the subsequent propagation of these particles through detector materials.
- Account for various stochastic processes such as scattering, decay, and absorption.

The strength of MC methods lie in their ability to incorporate detailed physics models, ranging from basic conservation laws to sophisticated interaction cross-sections, into a framework that can statistically reproduce experimental outcomes. However, the complexity of these simulations often results in significant computational demands, even more-so in the HL-LHC era.

To mitigate the strain on computational resources, ATLAS employs various fast-simulation tools that are capable of simulating different regions of the detector. The most mature of these tools is the fast calorimeter simulation, as the calorimeter requires a large portion of the simulation CPU. The work presented in this report aims to improve the physics performance of a fast-simulation tool which simulates the inner detector, called FATRAS. This tool is projected to be an integral part of the High Luminosity upgrade, as the inner detector in the next-most CPU-intensive part of detector simulation.

The way in which the physics performance is enhanced is by better modelling how photons interact with the detector material. There are several processes that photons can undergo, the key ones being Compton scattering, photon conversion and the photo-electric effect. Before the work presented in this report, the fast simulation of the inner detector only included photon conversions, and here, the implementation of Compton scattering is attempted.

A reasonable next step is to provide a brief summary of useful nomenclature and the physics of Compton scattering, before describing the ATLAS simulation framework in more detail.

2.4 Relativistic kinematics at the LHC

A short description of the convention used at ATLAS is required, along with some common terms and relations for relativistic kinematics. Much of the analysis presented uses the quantities described below.

2.4.1 ATLAS coordinate system

The coordinate system used in this report mimics the ATLAS standard [2]. A right-handed coordinate system is used with its origin at the interaction point (IP) of the two beams. The IP is in the centre of the of the detector, with the z-axis in the direction of the beam pipe. The x-axis is defined as the direction from the IP to the centre of the LHC ring, and the y-axis points upwards. In the transverse plane, cylindrical coordinates (r, ϕ) are used, where ϕ is the azimuthal angle around the z-axis. The quantity p_T is defined as the component of momentum in this transverse plane.

The momentum of particles are typically described using quantities which are defined relative to the beam axis; the pseudorapidity, η, the azimuthal angle, ϕ, and the transverse momentum p_T. Below is a more detailed description of the pseudorapidity η, and how to extract Cartesian momentum and energy from these quantities (η, ϕ, p_T), which constitute more natural choices for describing particle kinematics in collider experiments.

2.4.2 Pseudorapidity and angular separation

The pseudorapidity is a function of the polar angle to the beam axis, describing how forward or sideways the particle moves [13]. It is defined as

$$\eta = -\ln\left[\tan\left(\frac{\theta}{2}\right)\right], \tag{1}$$

where θ is the polar angle measured from the beam axis. A polar angle is taken such that a particle moving parallel to the beam axis has $\theta = 0°$ or $\theta = 180°$ and perpendicular to the beam is $\theta = 90°$.

The pseudorapidity is a frequently used kinematic quantity in HEP. This is because most particles are found at low polar angles, so the use of the natural logarithm means that the number density of particles per unit η is uniformly distributed.

Given these quantities, the angular separation between two particles is typically defined as the distance on the pseudorapidity-azimuthal angle plane:

$$\Delta R = \sqrt{(\Delta\eta)^2 + (\Delta\phi)^2}. \tag{2}$$

2.4.3 Energy and momentum in the Cartesian plane

To relate (η, ϕ, p_T) to the momentum and energy of particles in the Cartesian plane, the following relations can be used.

$$p_x = p_T \cos\phi, \tag{3}$$

$$p_y = p_T \sin\phi, \tag{4}$$

with the longitudinal component obtained from the pseudorapidity:

$$p_z = p_T \sinh\eta. \tag{5}$$

The total momentum is then

$$p = \sqrt{p_T^2 + p_z^2} = p_T \cosh \eta. \tag{6}$$

Finally, with the relativistic energy-momentum relation, the particle with mass m has energy E:

$$E = \sqrt{p^2 + m^2} = \sqrt{(p_T \cosh \eta)^2 + m^2}\,. \tag{7}$$

Now that some standard properties and definitions have been declared, the theoretical background of Compton scattering is presented.

2.5 Compton scattering

Understanding how photons interact with matter is crucial for the accurate modelling of physics in the detectors. As previously stated, the aim of this report is to include the modelling of Compton scattering into the FATRAS physics package. Here, the underlying physics principles of Compton scattering are considered.

2.5.1 The Compton effect

Compton scattering describes the inelastic collision between a photon and a loosely bound electron [14, 15]. The result is a photon of reduced energy and an ejected electron.

$$e + \gamma \rightarrow e + \gamma' \tag{8}$$

At the energy scales of the LHC, it is reasonable to consider incoming photons with GeV energies. As such, it is a reasonable approximation to call the electron free and at rest.

The shift in energy and wavelength due to Compton scattering can be written as a function of the scattering angle θ:

$$\lambda' - \lambda = \frac{h}{m_e c^2}(1 - \cos(\theta)) \tag{9}$$

$$\frac{1}{E'} - \frac{1}{E} = \frac{1 - \cos(\theta)}{m_e c^2}, \tag{10}$$

where $(\lambda, \lambda'), (E, E')$ are the wavelengths and energies of incident and scattered photons, respectively. With some rearranging:

$$1 - \cos(\theta) = \frac{m_e c^2}{E} \frac{(1 - \epsilon)}{\epsilon}, \tag{11}$$

where $\epsilon = E'/E$.

2.5.2 The Thomson limit and cross-section

In the low-energy limit of Compton scattering, where the electron rest mass is much larger than the photon energy, classical electrodynamics can describe the process [15]. In this energy regime, the differential cross-section is independent of the scattering angle. This is described by the Thomson formula [16].

First, it is useful to define the classical electron radius, r_0, as it is referenced frequently in the remainder of the report.

$$r_0 = \frac{e^2}{4\pi\varepsilon_0 m_e c^2}, \tag{12}$$

where m_e is the electron rest mass, e is the elementary charge, ϵ_0 is the vacuum permittivity and c is the speed of light. It follows that the Thomson cross-section is

$$\sigma_T = \frac{8\pi}{3} r_0^2 \approx 6.652 \times 10^{-29}\,\mathrm{m}^2. \tag{13}$$

Later in the report, this is used as a normalisation factor for Compton scattering events as it represents the classical limit of the scattering process.

2.5.3 The Klein-Nishina distribution

The theoretical description of the scattering is based on the Klein-Nishina (KN) distribution [15]. Assuming the electron is initially free and at rest, it describes the probabiltiy of Compton scattering as a function of incident angle and energy.

Importantly, the distribution can be split into differential and total cross-sections. The total cross-section describes the overall probability of a Compton scatter occurring, given the properties of the incoming photon. In contrast, the differential cross-section describes the probability distribution of the scattered photon's energy and angular properties. By sampling from both levels of the KN distribution, the MC methods described in the following sections should reliably reproduce the scattering process, enabling a realistic simulation of this flavour of photon interactions.

We begin with the differential cross-section:

$$\frac{d\sigma}{d\Omega} = \frac{r_0^2}{2} \left(\frac{E'}{E} \right)^2 \left(\frac{E'}{E} + \frac{E}{E'} - \sin^2\theta \right), \tag{14}$$

where r_0 is the classical electron radius, E and E' are the energies of the incident and scattered photons, respectively and θ is the scattering angle.

This quantifies the likelihood for a photon to scatter off an electron into a specific solid angle [14, 17]. When implementing Compton scattering into the fast-simulation software, the simulated angular and energy distributions of outgoing particles from an interaction should closely match the KN differential cross-section.

Moving to the total cross-section σ_{KN}: it is obtained by integrating Equation 14 over all solid angles and is a function of incoming photon energy E.

$$\sigma_{KN}(E) = \int_0^{\pi} \frac{d\sigma}{d\Omega}(E, \theta)\, d\Omega. \tag{15}$$

Equation 15 should be used if one wishes to model Compton scattering more completely. This report initially uses a flat rate for the total cross-section to simplify the implementation. In reality, the cross-section falls as a function of incoming photon energy, making Compton scattering more likely at smaller energy scales.

Combined, these formalisms provide the foundation for implementing Compton scattering into FATRAS. Our attention now shifts to the simulation framework within which this report is based.

3 ATLAS simulation basics

This section aims to provide more context for how the simulation packages available to ATLAS vary, and the purpose of each one. To do so, the ATLAS software framework Athena is introduced, followed by a description of the toolkits at the collaboration's disposal.

3.1 Athena framework

The ATLAS software framework, Athena [18], is built on the Gaudi architecture [19, 20] and provides interfaces for modules at various levels of the programmes operation. A full description of Athena is provided in [21]. Athena permits the use of common interfaces and modules, and FATRAS, the fast simulation tool upon which this report is based, is fully embedded within this `C++` framework [9].

All simulations presented in this report were done using a local version of Athena. Within this framework, code can be developed and tested before being merged with the public version used by the rest of the collaboration. One of the aims of this report is to validate the new implementation of physics effects enough for it to be circulated into the main branch of FATRAS.

Different simulators can be chosen, depending on what the aim of the simulation is. Below is a description of the two main modes of simulation used in this work, Geant4 and FATRAS, and how they might both be used in one study with the Integrated Simulation Framework.

3.2 The Integrated Simulation Framework (ISF)

Many physics studies require large MC samples yet only demand high precision simulation for specific regions or particle types. The ISF [22, 23] permits a flexible combination of the various simulation techniques available to ATLAS, each with a unique place on the spectrum between fast and accurate. By permitting different simulation approaches to be applied within even the same event, simulations become significantly more efficient, as there are minimally wasted computational resources. At the accurate end of this spectrum is Geant4, described below.

3.3 Geant4

Geant4 [3, 4, 24] is a toolkit that aims to be the industry standard of the simulation of particle transport and radiation through matter. Its applications are vast, from medical and nuclear physics, space and radiation science, through to High Energy Physics at the LHC. Geant4 provides up-to-date physics models and infrastructure for any user to model and simulate their own detector, providing a versatile simulation package which can be used to validate experimental data and draw physics conclusions or to design future detectors and predict their performance.

Many HEP collaborations have developed sophisticated models of their own experiments, and ATLAS is no exception. The ATLAS detector is constructed fully in the Geant4 format, while Athena takes care of the recording and analysis of particle characteristics [21]. Athena is also responsible for the logging of truth events[1] in the Monte Carlo simulations, meaning the record of particles that were *actually* generated in the simulation. This 'scoring' of particles is done only in detector volumes labelled as sensitive, so the output of the simulation can be as close as possible to the true output of the detector.

3.3.1 Physics Lists in Geant4

Every simulation of the detector has a specified list of physics it adheres to. This is an essential part of the toolkit as it permits the isolation of certain particles and processes.

With Geant4 simulations, this can be done using reference physics lists which package the particles to be used in the simulation together with the specific physics processes assigned to them[2]. For instance, many of the simulations that were run for this study involved only electro-magnetic (EM) processes and further, the ability to enable only Compton scattering among these EM processes is a useful feature.

[1] During event generation and detector simulation, a log of "truth" events are recorded. In simulation, truth level information represents our theory, and provides us with information that we then try to reconstruct using the actual measurement from our detectors. Differences between reconstruction and truth may suggest differences in physics!

[2] This work was done using an altered version of the `QGSP_BERT_MuBias` physics list.

3.4 Fast ATLAS Tracking Simulation (FATRAS)

In contrast to Geant4, FATRAS is a fast simulation engine of the ATLAS tracking system, including both the inner detector and the muon system [9, 10, 12]. It is designed to model the dominant effects of traversed detector material on particles. These effects include multiple scattering/ionisation loss, bremsstrahlung, hadronic interactions and photon interactions. FATRAS has also been used as a tool to explore alternate detector geometries [25] and inform design decisions made by the ATLAS collaboration.

FATRAS uses a simplified reconstruction geometry based on thin layers rather than the full detector volumes, as well as employing simplified physics parametrisations [9, 10]. This controlled simplification reduces computing time significantly while maintaining a high level of agreement with Geant4-based full simulation. A visualisation of this simplified geometry can be seen in Figure 1.

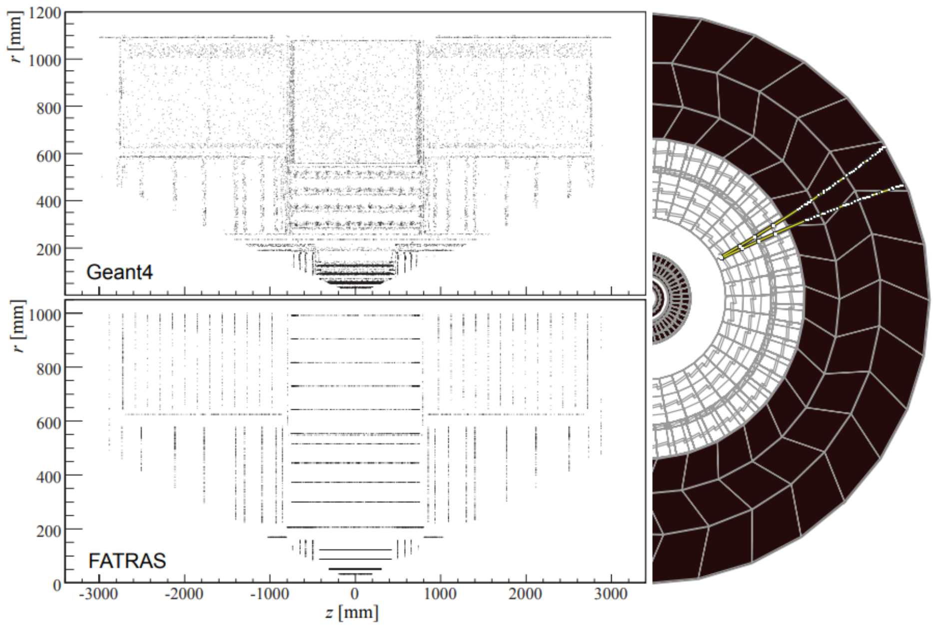

Figure 1. A comparison between the full Geant4 geometry (top) and the simplfied ATLAS reconstruction geometry (bottom) used in FATRAS. This figure was made using positional information of simulated photon conversions. FATRAS' approximation of the detector as thin layers can be visualised in the bottom panel. This reduces the computational expense while preserving key physics responses. Figure 3b) from [10].

While it is promising that there are faster tools being developed for the generation of MC events, for FATRAS to replace the full Geant4-based simulation and be deployed in Run 4, the physics performance of the tool needs to be of a high standard. To reach this standard, all the prominent physics effects must be modelled, hence the motivation for this project.

FATRAS is structured as a collection of modular `C++` components within the Gaudi/Athena framework. Each modelled physics effect - hadronic interactions, electron bremsstrahlung, multiple scattering, photon conversions, and now Compton scattering - has a dedicated 'Tool' which implements the relevant physics logic. By keeping these tools modular, FATRAS can apply interactions sequentially as a particle travels through the simplified detector layers.

Some modules act as updators or steppers. Most notably, the `TransportTool` handles the raw geometrical stepping of the particle, and calls the `McMaterialEffectsUpdator` to apply the material interaction at a given step. The job of the `McMaterialEffectsUpdator` is to query the `ProcessSamplingTool` to decide which process should be applied, and then call the specialised Tool which implements that physics process. For example, this work highlights the development of the `ComptonScatteringTool`, which has been written to model the Compton scattering process. As long as the KN total cross-section is not implemented, the `ProcessSamplingTool` will simply invoke this Tool 4% of the time, a value initially suggested by the FATRAS developers.

3.5 MC Production Chain

Now that the various tools at our disposal have been explored, a brief description of the MC production chain is presented. This should explain the order in which simulations are run. For a full review, please consult [21]. This chain explains the process by which simulated data is generated, ready for the analysis presented in Section 5.

- **Event Generation:**
  - The production chain starts with event generation, where the four-momenta of particles are created. In this work, photon samples are produced using ParticleGun, an external event generator.
- **Detector Simulation:**
  - The simulation models the interactions of generated particles with the detector material. In sensitive volumes, these interactions produce 'hits' that represent the detector's response[3].
- **Digitisation and Reconstruction (Full Chain):**
  - Typically, the hits are passed through digitisation algorithms, which convert them into a format mimicking the detector readout.
  - Reconstruction algorithms then process these digits to build high-level objects such as tracks, clusters, and vertices for detailed physics analysis.
- **Validation:**
  - In this work, instead of running the full digitisation and reconstruction chain, a rapid validation process is used.

[3]The Python script to run this in Athena is `Sim_tf.py`

– The validation tool[4] processes the hits to generate histogram files. These histograms are compared against expectations from full Geant4-based simulations to ensure that basic distributions and observables are consistent.

Finally, a closer look at the structure of the developed `ComptonScatteringTool` can be explored.

4 Methods

This section has two aims. The first is to outline the method in which the differential cross-section that describes Compton scattering has been implemented and analysed. The second aim is to discuss a proposed parametrisation of the KN total cross-section. The results corresponding to each of these points are presented in the next section, all compared to the relevant theoretical predictions.

4.1 Implementation of the `ComptonScatteringTool` within FATRAS

Figure 2 illustrates how the `McMaterialEffectsUpdator` acts as a centralised updator module. The class will branch out to call the required tools depending on the decision of which process the particle will undergo. To run FATRAS simulations with altered physics, such as forcing every photon to undergo Compton scattering, the afore-mentioned `ProcessSamplingTool` can be modified such that whenever a photon is interacting with a detector layer, the `ComptonScatteringTool` is called exclusively.

Importantly, the changes made to FATRAS physics processes should be replicated when producing Geant4 data as a confirmation. This is done by altering the physics lists in Geant4.

The new `ComptonScatteringTool`, called by the `McMaterialEffectsUpdator`, undergoes the following key steps:

- Initialise and retrieve the necessary service tools (e.g., random number generator, truth record service, validation tools).
- Calculate the energy and direction of the scattered photon and of the recoiling electron by implementing an algorithm which samples from the differential KN cross-section.
- Releases the scattered photon and ejected electron into the stack of truth particles.

Below is an outline of the functionality of the developed Compton scattering class.

[4]Executed in Athena with `simValid_tf.py`

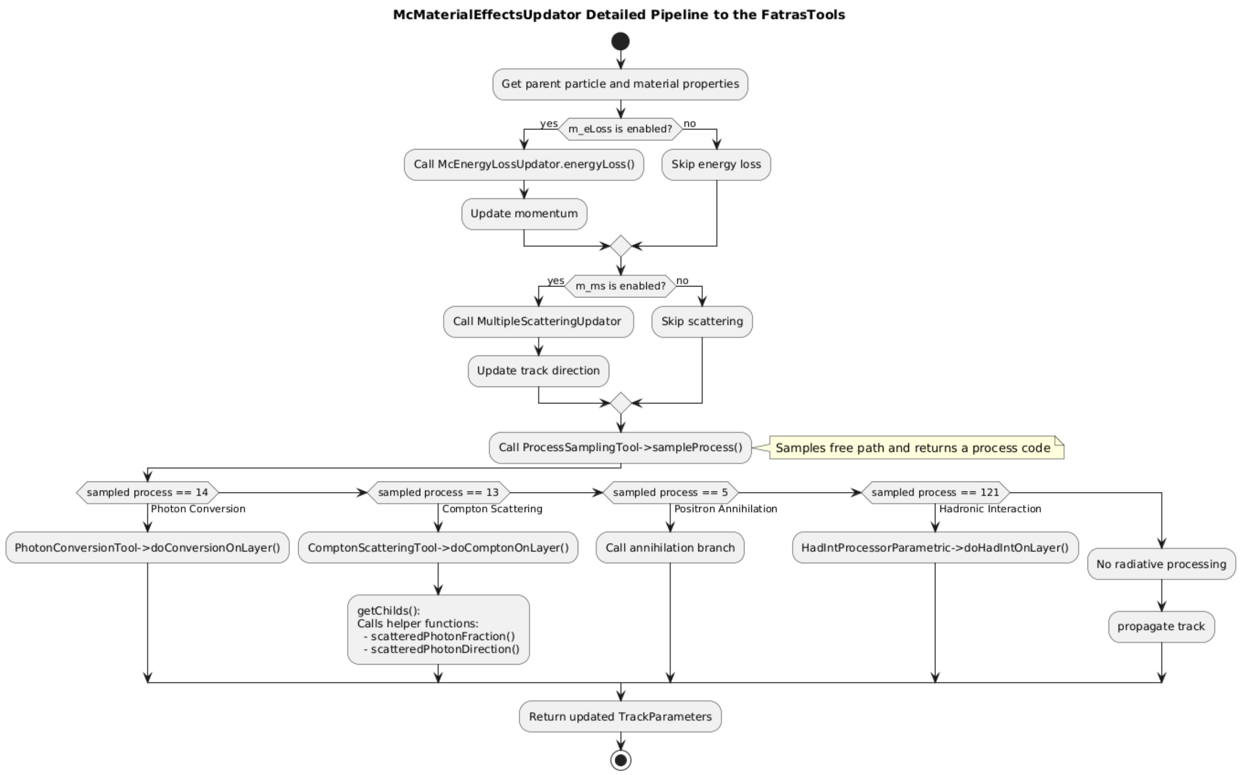

Figure 2. A UML diagram showing the workflow between the updator class `McMaterialEffectsUpdator` and the various tools used to model different processes. This class is responsible for calling the appropriate physics processes when handling the particle-material interactions.

4.1.1 Key function calls

The publicly accessible method `doComptonOnLayer()` is the entry point for the simulation of Compton scattering on a detector layer. It receives a pointer to the parent photon (which is an `ISFParticle`) and the parent's position and momentum via a `Trk::NeutralParameters` object. Within the `ComptonScatteringTool`, `doComptonOnLayer()` does the following:

1. **Initial four-momentum construction:** The parent photon's four momentum is constructed from the provided `Trk::NeutralParameters`.

2. **Sampling of scattering variables:** The function `scatteredPhotonFraction()` is called and a rejection sampling algorithm is used to sample two quantities from the differential KN distribution:

   - The energy fraction ϵ that the scattered photon carries, where $E_{\text{scattered}} = \epsilon\, E_\gamma$.
   - The scattering angle θ.

3. **Direction update:** With the angle θ computed, the method `scatteredPhotonDirection` applies a rotation (with an additional random azimuthal angle ϕ) to the parent photon direction, returning the direction of the scattered photon.

4. **Recoil electron four-momentum:** Using energy-momentum conservation, the ejected electron's four momentum is computed by subtracting the scattered photon's four momentum from the parent's four momentum (and accounting for the electron's rest mass).

5. **Child generation:** Finally, the method `getChilds()` is called to create two new `ISFParticle` objects, representing the scattered photon and the recoil electron.

This sequence of operation encapsulates the physics of the interaction, with tracking of all daughter particles and consistent use of conservation laws. Now, a closer look at the sampling algorithm employed is warranted.

4.1.2 Sampling algorithm in `scatteredPhotonFraction()` and the Klein–Nishina distribution

Given that the energy scales of the incoming photons are much higher than the electron's ionisation potential, the absorbing electron is considered to be free [26]. Further, ignoring the binding effects of atomic electrons, the scattering of an energetic photon by an electron can be described as a two-body collision. As such, the combined composition and rejection sampling techniques used in Geant4 [27], first set out by [26, 28] can be utilised. The implementation in `scatteredPhotonFraction()` is as follows:

1. **Backscattering threshold calculation:** The threshold ϵ_0 is computed as

$$\epsilon_0 = \frac{m_e}{m_e + 2E_\gamma}, \tag{16}$$

   where m_e is the electron mass and E_γ is the energy of the incident photon. The sampled ϵ values must lie between $[\epsilon_0, 1]$.

2. **Definition of sampling coefficients:** Two coefficients are defined to set up the candidate distributions:

$$\alpha_1 = \ln\left(\frac{1}{\epsilon_0}\right) \quad \text{and} \quad \alpha_2 = \frac{1-\epsilon_0^2}{2}.$$

   These coefficients determine the probabilities of sampling from two candidate distributions, denoted f_1 and f_2. These functions mimic the energy dependence predicted by the differential KN distribution (in Equation 14).

3. **Sampling candidate ϵ value:** A uniform random number is used to decide whether to sample ϵ from:

   - **Branch f_1:** With probability $\frac{\alpha_1}{\alpha_1+\alpha_2}$, sample

$$\epsilon = \epsilon_0^{r'},$$

     where r' is a uniformly distributed random number.

- **Branch f_2:** Otherwise, sample

$$\epsilon = \sqrt{\epsilon_0^2 + (1 - \epsilon_0^2)\, r'}.$$

4. **Scattering angle computation:** Once a candidate ϵ is determined, the algorithm uses relations derived from energy-momentum conservation to compute the scattering angle θ. First, the variable

$$t = \frac{m_e}{E_\gamma} \frac{1 - \epsilon}{\epsilon},$$

   and subsequently,

$$\sin^2 \theta = t(2 - t).$$

   The scattering angle is then given by:

$$\theta = \arcsin\left(\sqrt{\sin^2 \theta}\right).$$

5. **Rejection Sampling Criterion:** Finally, a rejection function $g(\epsilon)$ is constructed so that the accepted samples represent the true KN distribution:

$$g(\epsilon) = 1 - \frac{\epsilon \sin^2 \theta}{1 + \epsilon^2}.$$

   A second uniformly distributed random number is generated, and the candidate values are accepted if $g(\epsilon)$ exceeds this number.

4.1.3 Proper relativistic treatment of interacting particles

Careful consideration should be given to treating the electron's momentum in a fully relativistic manner [17]. Instead of subtracting the scattered photon's direction from the incoming photon's direction, the electron four-momentum is considered:

$$p_e = (p_{\gamma i} + m_e) - p_{\gamma f},$$

where m_e - the rest mass of the electron - is the electron's initial momentum and $p_{\gamma i}$ and $p_{\gamma f}$ are the initial and final photon four-momenta, respectively. This approach correctly accounts for proper conservation of four-momenta during Compton scattering.

4.1.4 Current implementation and future directions

As explained in subsection 2.5, there are two levels at which the KN distribution can be used. Currently, only the differential KN cross-section is implemented into FATRAS, meaning that the rate at which Compton scattering events occur are fixed at 4%, regardless of the incoming photon's energy. As previously mentioned, this number is used due to a suggestion by the FATRAS developers, and will soon be replaced by a better representation of the physics.

This is clearly a pitfall of the implementation at present, and represents future work. The proposed way forward is to parametrise the cross-section as a function of the incident energy, instead of sampling directly from the theoretical cross-section, as this involves an expensive integral. This is explored in more detail later in the report.

4.2 Using truth-level information to extract quantities used for analysis

Note that for all analysis performed in this report, the incident photon samples were uniformly distributed with a p_T range of $[5, 15]$ GeV and η range of $[-2.5, 2.5]$. These were made using ParticleGun, an external event generator.

Four key pieces of information output by the simulation are used to analyse the data generated by Geant4 and FATRAS simulations; the particle ID, the pseudo-rapidity, η, the azimuthal angle ϕ and the transverse momentum p_T. In a null event, only the incident photon will be saved as a truth-level particle. In FATRAS - where the total cross-section for scattering can be artifically set to 100% - this occurs when the released electron has less than 50 MeV of energy. On the other hand, in Geant4, the null event is significantly more frequent, because the total cross-section is implemented in full, meaning that Compton scattering is called less frequently.

Given this information, only events with valid electrons released are considered to be Compton scattering events. After this cut, the four-momenta of the incident photon and the first produced electron are computed with `pylorentz`. This Python package performs the relativistic kinematics calculations outlined in subsection 2.4, reconstructing the four-momentum

$$p^\mu = (E,\ p_x,\ p_y,\ p_z) \tag{17}$$

for every particle of interest. These quantities can then be extracted, ready for analysis.

4.3 Implementing the KN total cross-section

As discussed in the background subsection 2.5, an implementation of the total cross-section would in principal involve an integral over the entire polar angle θ for each incoming photon. While the implementation is important for capturing all of the physics, this would be very computationally expensive. As such, there is strong motivation to develop a parametrisation of the integral. This should be a linear combination of physically motivated terms that capture the shape of the distribution.

To achieve this, the Thomson cross-section introduced in Equation 13, is used as a normalisation factor in the model. The model will be as follows:

$$\sigma(E) = \sigma_T \sum_{i=0}^{n} a_i \phi_i(x), \tag{18}$$

where x is the dimensionless energy variable $x = \frac{E}{m_e c^2}$, σ_T is the Thomson cross-section and a_i are the weighting coefficients to be determined. The functions $\phi_i(x)$ are designed to capture the energy dependence of the cross-section. These are detailed in Table 1, along with the physical interpretations of each chosen function.

Index i	Basis Function $\phi_i(x)$	Physical Motivation
0	1	Constant for normalisation
1	$\log(1+2x)$	Logarithmic energy dependence
2	$\frac{1}{1+2x}$	Models the reduced cross-section at high energies x
3	$\frac{1}{(1+2x)^2}$	Allows for sharper decay at high energies x
		Extended Model Terms
4	$\sqrt{1+2x}$	Introduces a moderate scaling term with energy
5	$\log^2(1+2x)$	Curvature of logarithmic dependence
6	$(1+2x)^{-3}$	Even higher-order decay effects
7	$\phi_1 \cdot \phi_2$	Mixing term between logarithmic and inverse dependencies

Table 1. Chosen functions $\phi_i(x)$ for the parametrisation of the KN total cross-section. The first four terms were used initially in the simple model, and the method was refined with the higher-order, extended terms.

These basis functions are then passed to a linear regression model using the `scikit-learn` module `LinearRegression`. This module applies the least squares formula to minimise the sum of squared residuals

$$\min_{\mathbf{a}} \|X\mathbf{a} - \mathbf{y}\|^2, \tag{19}$$

where $\mathbf{X}$ is the design matrix where each row is an energy value x_j and each column is a basis function. $\mathbf{y}$ on the other hand is the target vector normalised by σ_T

$$\mathbf{y} = \left[\frac{\sigma_{KN}(x_1)}{\sigma_T}, \frac{\sigma_{KN}(x_2)}{\sigma_T}, \ldots, \frac{\sigma_{KN}(x_M)}{\sigma_T}\right]^T. \tag{20}$$

This method has been tested and the results are shown at the end of Section 5.

5 Results and Discussion

There are four key results which are explored below. First, a demonstration of physical understanding for the theoretical KN cross-section as a function of theta. Next is a demonstration of the validity of the sampling algorithm described in subsection 4.1. This study is performed independently of the FATRAS or Athena framework, to avoid any complications and act as a benchmark for the results obtained by the FATRAS simulation. In the third section, the FATRAS simulation results are presented and compared to both the 'clean' sampling results and the full Geant4-based simulation. Both FATRAS and Geant4 simulations were performed with an altered physics list containing only Compton scattering. Finally, the proof of principle for the parametrisation of the total cross-section is presented. This is promising work but has not yet been implemented or validated within FATRAS.

5.1 Understanding the differential cross-section predictions

Before discussing the implementation of the rejection and composite sampling technique used in Geant4 and now implemented in FATRAS, it is useful to examine the theoretical differential cross-section as a function of the scattering angle, θ.

For a given incoming photon with energy E, the photon frequency and wavelength can be computed using Planck's relation. A unique wavelength of the scattered photon is then given by the Compton shift equation, Equation 9, after which the ratio $P = \frac{\lambda}{\lambda'}$, (equivalent to the energy fraction $\epsilon = \frac{E'}{E}$ in Equation 14) is used. As a result, the differential cross-section is computed as:

$$\frac{d\sigma}{d\Omega} = f\, P^2 \left(P + \frac{1}{P} - \sin^2\theta \right), \tag{21}$$

where

$$f = \frac{(\hbar\,\alpha/(m_e\,c))^2}{2}\,.$$

f is half the square of the classical electron radius. Given the classical electron radius

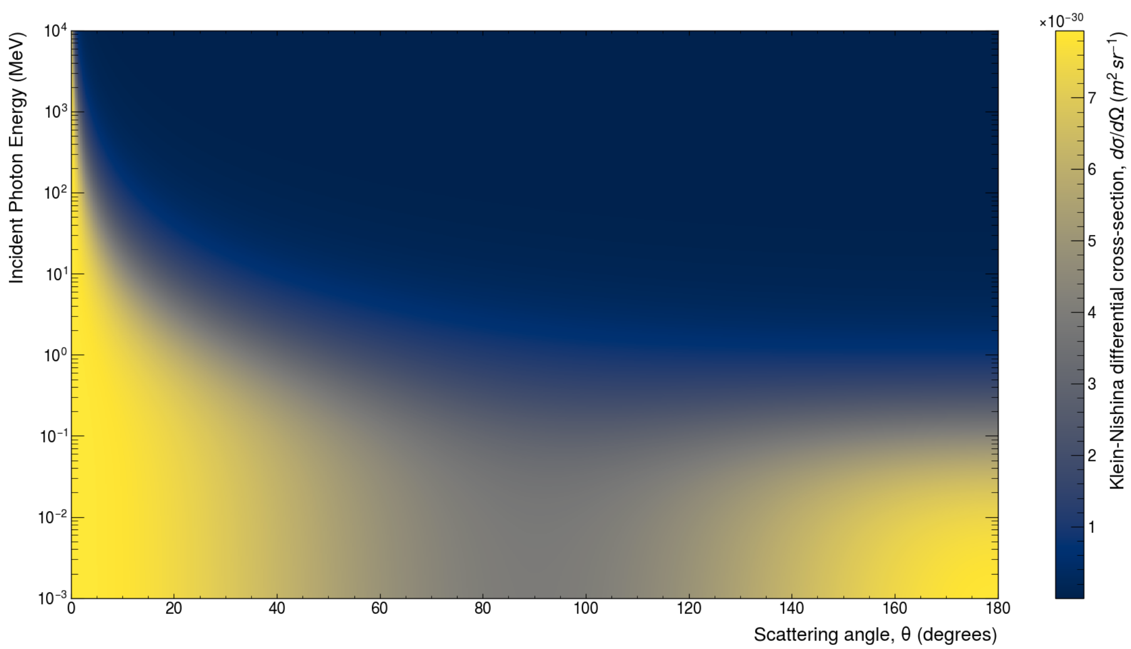

Figure 3. A 2D histogram showing the theoretical Klein-Nishina differential cross-section as a function of incident photon energy and scattering angle θ. The distribution illustrates the transition from forward-backward preference at low-energies, to the highly forward-peaked distribution seen at high ($\approx 10\,\text{GeV}$) incident photon energies.

squared r_0^2 sets the scale of the cross-section, it is expected to see $\frac{d\sigma}{d\Omega}$ on the order of $10^{-30}\,\text{m}^2$. Figure 3 shows the theoretical cross-section as a function of both incident photon energies and scattering angle θ.

At low energies ($O(1)$ keV), there is a forward-backward preference in scattering directions, with a dip present at 90°. This dip arises as a result of the $\sin^2(\theta)$ seen in Equation 21, where $\theta \approx 90° \Rightarrow \sin^2(\theta) \approx 1$ corresponds to a minimum in differential cross-section.

At high energies ($O(10)$ GeV), it is clear that there is a much stronger forward preference, with the cross-section dropping very quickly with the scattering angle.

To confirm this understanding, Figure 4 presents five incoming photon energies and similar to before, illustrates the respective theoretical cross-sections, presenting it on the polar plane. This helps visualise the forward preference of the KN distribution for high energy photons, and the broader spread of low energy photons across different scattering angles, causing back-scattering to occur more often.

Generally, small θ implies $\epsilon \approx 1$, as most of the incident energy is taken away by the scattered photon. Combined, these figures help understand the results below, showing what to expect from the full implementation.

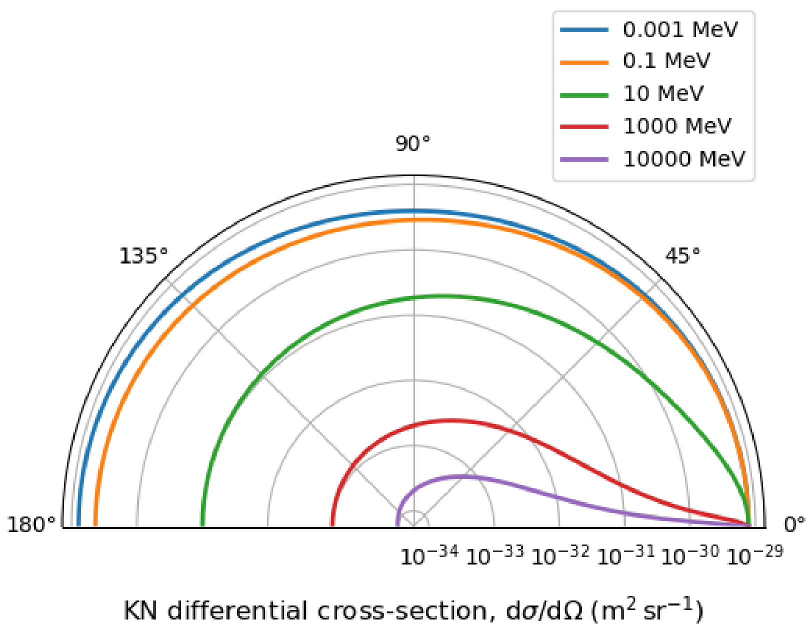

Figure 4. Differential cross section $\frac{d\sigma}{d\Omega}$ as a function of scattering angle (in degrees) for given photon energies from 1 KeV to 10 GeV. Plotted in the polar plane to aid visualisation. The strong forward preference of high energy photons, compared to the more symmetric keV photons is highlighted by the polar representation.

5.2 Validation of sampling mechanism

As discussed in subsection 4.1, a rejection sampling algorithm is employed to generate pairs (ϵ, θ) from the KN differential cross-section. An analysis of this algorithm outside of FATRAS

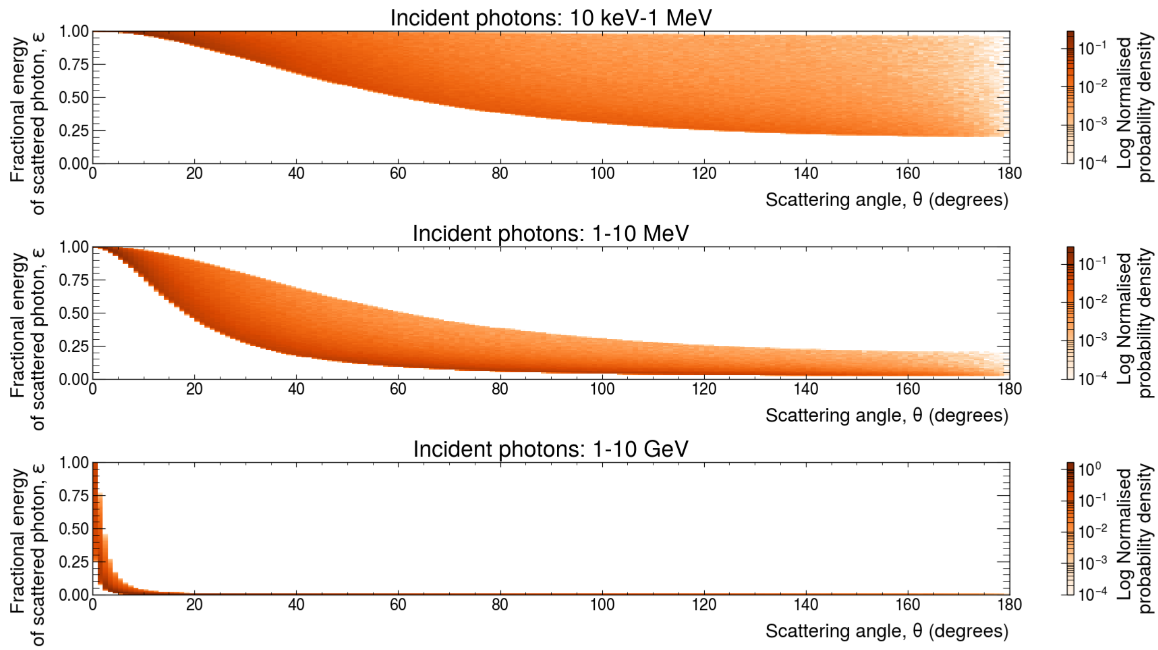

Figure 5. 2D histograms of the fractional energy carried away by the scattered photon ($\epsilon = E_{scattered}/E_{initial}$) versus the scattering angle θ, analysed at three different energy ranges. These distributions are made using 1 million photon samples randomly distributed between the energies noted in the subplot titles. The sampling algorithm used here is the same as the one implemented into FATRAS, described in subsection 4.1.

is performed, with the expected distributions for ϵ, θ shown in Figure 5. Random photon samples at different energy scales were passed into the full sampling algorithm, generating and accepting candidate scattered photons, and computing the resulting ϵ and θ pairs.

The frequency of each sampled pair is plotted as a log normalised distribution.

- In the top panel, the presence of the lower limit of ϵ at ≈ 0.2 is consistent with the fact that ϵ is sampled between $[\epsilon_0, 1]$, where ϵ_0 is the backscattering threshold. Using Equation 16, introduced when describing the `ComptonScatteringTool`, the minimum energy a 1 MeV photon could have is $\frac{0.511[MeV]}{(0.511+2)[MeV]} \approx \frac{1}{5} = 0.2$. These values are consistent and a properties of the sampled distribution can be described physically.

- In the middle panel, the incident photons now have a higher energy than the electron mass, and there is a much smaller limit on the smallest sampled ϵ values. It is also evident that the distribution becomes more forward peaked, which aligns with the theoretical expectation. This can be seen by noticing the larger probability densities for smaller angles.

- Lastly, the bottom panel shows a strong forward scattering preference with ϵ falling off very quickly as a function of scattering angle. Importantly, the probability density (cross-section) does not got to zero for higher scattering angles, but the sampled ϵ

values are forced to be very small, due to the relative energy difference between the electron rest mass and the incident photon.

This figure illustrates the results of checking the physical consistency of the sampling algorithm. Clear trends are present between the variables, and these are in agreement with our expectations based on comparisons to the electron mass.

5.3 Comparing Compton scattering and photon conversion events simulated in FATRAS

As further validation that the Compton effect is being modelled correctly, a comparison is drawn between Compton scattering and photon conversion events simulated in FATRAS. Using the p_T imbalance and the spatial separation between the final state particles of each interaction, certain predictions can be made on how each distribution should look.

5.3.1 Predicted results

In photon conversions, the electron-positron pair will be created exactly at the site of the photon, so zero spatial separation between the electron and the positron is expected. In terms of the transverse momentum imbalance, the electron and positron are produced isotropically, so a flat distribution is expected.

In Compton scattering, the distribution of angular separation between final state particles (γe^-) is expected to be broader than that of photon conversion, as the scattering can occur at a distance to the interaction point. For the p_T imbalance, as previously seen (in the lowest panel of Figure 5), for any scattering angle larger than 10 degrees, ϵ will be extremely small. This means that the calculated momentum imbalance should be significant and peaked near 1, as the electron will be taking almost all of the energy away from the interaction.

One complicating factor of the p_T imbalance is that FATRAS imposes a 50 MeV minimum momentum threshold on the particles saved. It should be noted that the criterion for identifying a Compton event is that a truth electron is saved by the simulation. As a result, many events record the electron while missing the scattered photon. Thus, to visualise the large p_T imbalance due to Compton scattering, one must calculate the final state photon p_T via a subtraction of the ejected electron's energy from the incident photon's energy.

5.3.2 Simulated results

Table 2 is a summary of the above arguments, concisely presenting the expected properties of the distributions. The distributions in Figure 6 align well with these expectations, suggesting that the implemented scattering process models the expected physics results well, and the results can be reasoned physically.

Feature	Photon Conversion ($\gamma \to e^+e^-$)	Compton Scattering ($\gamma e^- \to \gamma e^-$)
ΔR	All very close to 0, generated in same place	Broader, as it depends on scattering angle
p_T Imbalance	Flat, symmetric. Falls off at high imbalance due to minimum momentum threshold	Peaks at 1 only when disregarding minimum momentum threshold

Table 2. Summary of expected results when comparing photon conversion and Compton scattering.

The dashed vertical line in Figure 6 displays the calculated imbalance between the mean p_T value and a 50 MeV particle, aligning well with the observed dip in imbalance of the conversion dataset.

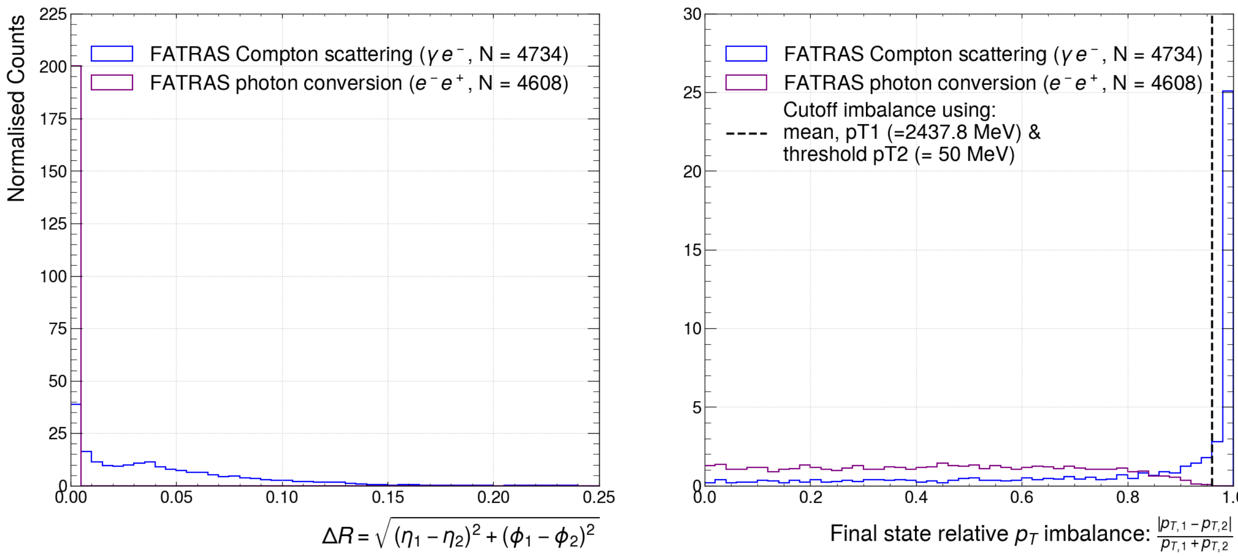

Figure 6. Normalised distributions of the angular separation ΔR (left) and the relative transverse momentum p_T imbalance (right) between final state particles in photon conversion (e^-e^+) and Compton scattering (γe^-) events simulated using FATRAS. The dashed vertical line in the right panel represents the expected imbalance when one particle has the mean energy and the other is at 50 MeV. Because 50 MeV is the minimum momentum cutoff in FATRAS, this accounts for the dip in p_T imbalance at values near 1.

5.3.3 Relation to KN total cross-section

Not that it was ever a doubt, but this analysis furthers the case for implementing the total cross-section of the Klein-Nishina distribution (the probability of calling Compton scattering as a function of incident photon energy). By doing so, a reduction in the number of events with valid electrons and invalid photons would be observed. This is because the total cross-section increases for lower energy incident photons. Again, as visualised in Figure 5, this would increase the probability of recording both final state particles, as there's higher probability to sample a larger ϵ value.

5.4 Compton scattering in FATRAS and Geant4

This subsection highlights an important result; the comparison of Compton scattering events simulated by Geant4 and FATRAS. While the previous results have been promising, Geant4 is used as the benchmark for physics simulations, so agreement between the two implementations is a strong validation of the method.

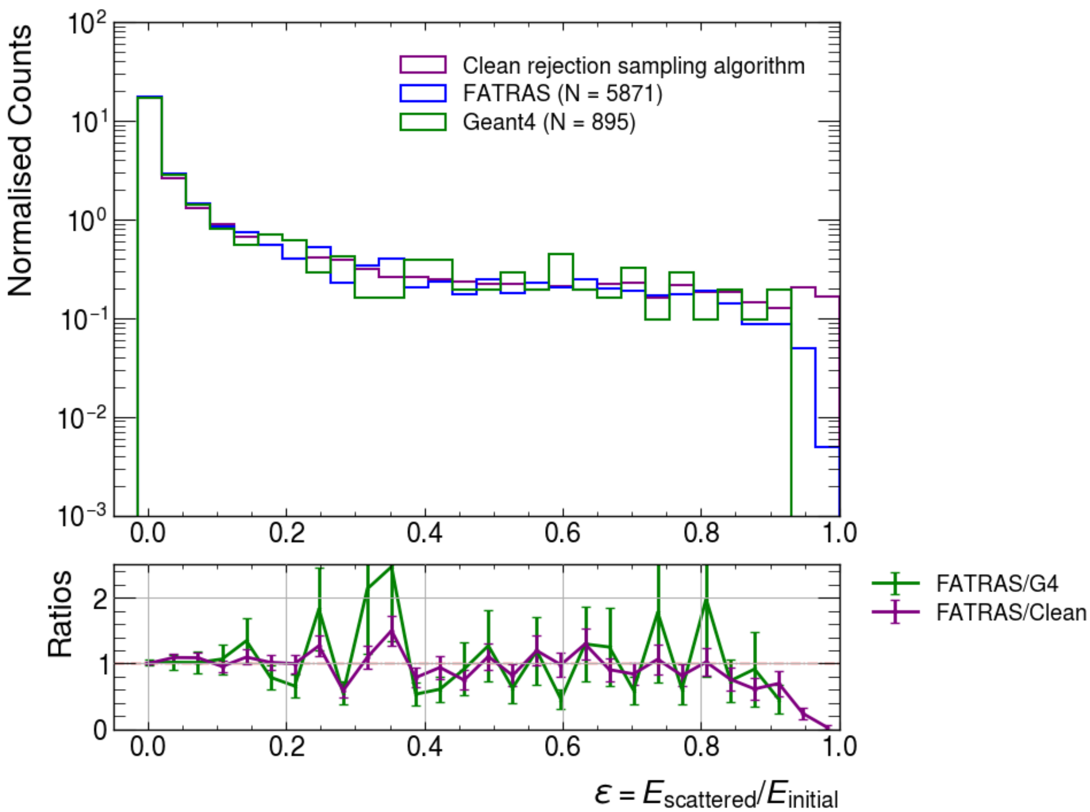

Figure 7. A histogram showing the fraction of energy a scattered photon carries away ϵ in Compton scattering events simulated using FATRAS (blue), Geant4 (green) and a standalone rejection sampling algorithm (blue). There is strong agreement between FATRAS and Geant4, quantified by a Kolmogorov-Smirnov test (KS statistic = 0.026, p-value = 0.646). This validates the physics performance of the implemented sampling method in FATRAS. The discrepancy at high ϵ is due to the 50 MeV minimum momentum threshold for recorded particles in FATRAS.

Figure 7 shows that there is strong agreement between the two distributions. The clean rejection sampling algorithm discussed in subsection 5.2 is included as a further confirmation.

This may suggest that the implementation of Compton scattering into the FATRAS framework has been successful. As such, a quantitative evaluation of the comparison is needed.

The Kolmogorov-Smirnov (KS) test is used to quantify the difference between the benchmark that is Geant4 and the FATRAS simulation.

The KS statistic measures the maximum difference between the cumulative distribution functions (CDFs) of the Geant4 and FATRAS samples. A small KS statistic implies the two CDFs are similar in shape. On the other hand, the p-value represents the probability that the differences in CDFs could have occurred by chance, meaning that a low score (say 0.05) would indicate a statistically significant difference between the two distributions.

The test on the two unbinned distributions of epsilon return a KS statistic = 0.026 and a p-value = 0.646. These suggest that the FATRAS and Geant4 ϵ samples could have been drawn from the same underlying distribution. Put otherwise, the CDFs of the two datasets are statistically similar.

5.4.1 Discrepancy at high epsilon

At high ϵ values, there is a clear discrepancy between FATRAS and the clean rejection sampling algorithm. This is again, a result of the minimum momentum threshold being enforced in FATRAS. The effect here is that at high ϵ, photons carry away all of the energy, so the electrons are left with too small a momentum to be released into the truth stack of particles. As such, the event is not identified as a Compton scatter, and it looks as if FATRAS predicts no sampled ϵ values near 1, so the ratio seen in the figure goes to zero.

5.5 Total cross-section

The results of the regression method outlined in subsection 4.3 are illustrated in Figure 8. The simple model, which utilises four basis functions, is capable of capturing the general shape of the theoretical cross-section, but shows significant deviations at energies above 10^3 MeV, with some evident lack of flexibility in the model for the middle regions.

In contrast, after incorporating the extra terms into the model, the ratio plot shows strong agreement across all eight orders of magnitude, with some slight deviation at energies close to 100 GeV. This confirms that the parametrisation presented does a good job at capturing the energy response of the KN total cross-section.

Importantly, the accuracy of the model is limited to the range of energies over which it was trained. It is clear that due to the limited expressiveness of the model, there may still be more physically motivated functions that would better capture the physics, ensuring that more nuances of the KN formula are accounted for. Further, the concept of fixed parametrisation introduces a rigidity that could be surpassed entirely with a more flexible neural network model. After attempting simple versions of multi-layer perceptrons (MLPs) and gradient boosted decision trees (GBDTs), the GBDTs are found to be more successful and easier to implement. GBDTs are good at handling non-linear forms without any pre-defined functional forms. This makes them a strong choice for creating a fast surrogate model of the total cross-section, and preliminary studies of them have proved successful.

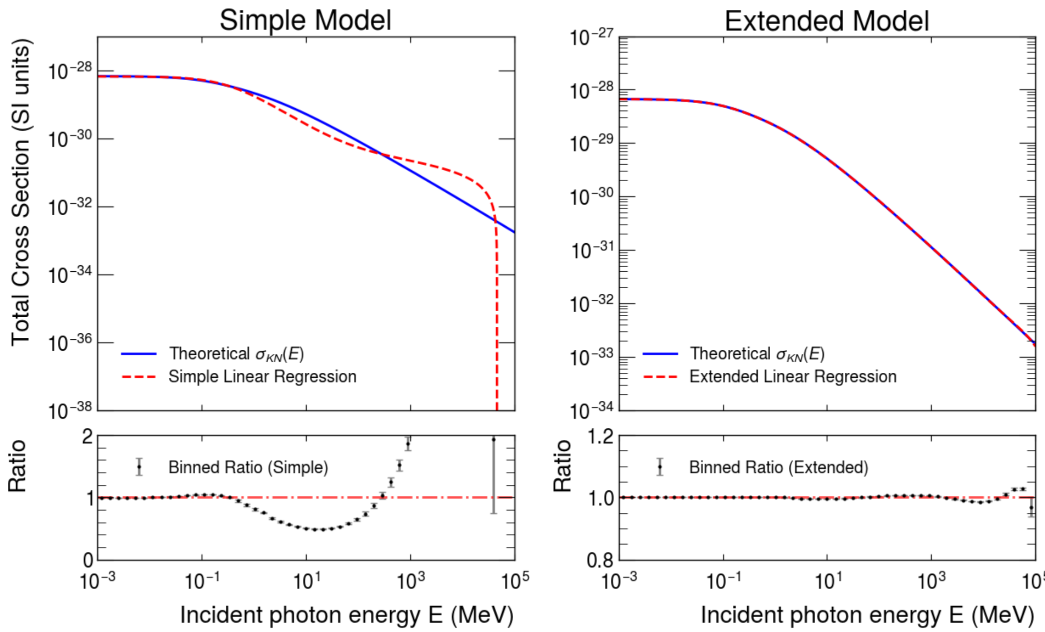

Figure 8. Comparison of the total Klein-Nishina cross-section with a simple and extended parametrised model spanning 8 orders of magnitude. On the left, the simple model shows a significant deviation at high energies and a lack of model flexibility in the central region, with the ratio of the fitted model to the theoretical prediction displayed in the lower panels. On the right, the additional basis functions lead to strong agreement across the energy range.

If deemed satisfactory, either this linear parametrisation or a more involved algorithm should replace the flat rate currently implemented in FATRAS. The validation of these replacements will involve ensuring the energy range they've trained over is sufficient, and comparing the results to Geant4 simulations.

6 Conclusion and Future Outlook

This report has presented the implementation and partial validation of the Compton scattering process into FATRAS. A complete implementation of Compton scattering into FATRAS would look as follows:

- Both the differential and integrated (total) Klein-Nishina cross-sections implemented.
- Benchmarking of both implementations' physics performance against Geant4.
- Benchmarking of both implementations' computational efficiency against Geant4.

As steps toward achieving this goal, clear demonstrations of theoretical expectations have been presented, and the `ComptonScatteringTool` has been developed and integrated into FATRAS. This tool utilises a sampling mechanism based on that of Geant4 to draw the scattered photon and electron properties from the differential KN distribution. This sampling mechanism uses Monte Carlo techniques to avoid the numerical integrals needed to directly invert the KN distribution, drawing instead from two simple, physically motivated functions. The physics performance of this tool has been validated against Geant4, with a Kolmogorov-Smirnov test suggesting the resulting distributions are statistically similar. Additionally, the results can be physically reasoned when compared to the behaviour of photon conversion within FATRAS, providing a physical basis for the shapes of simulated distributions. While this is a promising result that will improve the physics performance of FATRAS, the benchmarking of the speed of this simulated interaction is a necessary piece of information to be obtained. The results of the tests on computing time would inform whether a parametrisation/machine learning technique should be implemented to model the process instead of using the full sampling technique described in this report.

As for the total KN cross-section, a promising idea for the parametrisation of the theoretical expectation has been proposed and its validity has been demonstrated. Further studies of two machine learning techniques were attempted, with Gradient Boosted Decision Trees returning very promising results. This provides a framework for further research if the proposed parametrisation is deemed too inflexible. Further work lies in implementing and testing the proposed parametrisation within FATRAS. The accuracy of the implemented method can easily be tested by comparing the total number of Compton scattering events to those of Geant4, given the same incident photon sample.

As a result, the physics performance of FATRAS will be of higher standard, and it is one step closer to becoming a reliable part of the ATLAS Simulation toolkit in the upcoming High-Luminosity LHC era.

References

[1] ATLAS Collaboration. The ATLAS Experiment at the CERN Large Hadron Collider. *JINST*, 3(8), 12 2008.

[2] ATLAS Collaboration. The ATLAS Experiment at the CERN Large Hadron Collider: A Description of the Detector Configuration for Run 3. *Journal of Instrumentation*, 19(5), 5 2023.

[3] GEANT4 Collaboration. GEANT4 - A Simulation Toolkit. *Nucl.Instrum.Meth.A*, 506(3):250–303, 7 2003.

[4] T. Basaglia et al. Geant4: a Game Changer in High Energy Physics and Related Applicative Fields. 3 2024.

[5] ATLAS Collaboration. ATLAS upgrade for the HL-LHC. *Nucl.Instrum.Meth.A*, 1069, 12 2024.

[6] I Bejar A and L Rossi. HiLumi LHC Technical Design Report: Deliverable: D1.10. Technical report, CERN HL-LHC, 2015.

[7] S. Hamilton et al. The ATLAS Fast Track Simulation Project. 3 2011.

[8] R. Jansky. The ATLAS Fast Monte Carlo Production Chain Project. *J.Phys.Conf.Ser.*, 664(7), 2015.

[9] K. Edmonds, S. Fleischmann, T. Lenz, C. Magass, J. Mechnich, and A. Salzburger. The Fast ATLAS Track Simulation (FATRAS). *ATL-SOFT-PUB-2008-001, ATL-COM-SOFT-2008-002*, 3 2008.

[10] J. Mechnich. FATRAS-the ATLAS Fast Track Simulation project. In *J. Phys.: Conf. Ser. 331 032046*, 2011.

[11] M. Javurkova. The Fast Simulation Program of ATLAS at the LHC. *42nd International Conference on High Energy Physics (ICHEP 2024)*, 2024.

[12] A. Salzburger. *Track Simulation and Reconstruction in the ATLAS experiment*. PhD thesis, Innsbruck U., 2008.

[13] V.I. Goldanskiĭ, I.U.P. Nikitin, and I.L. Rozental. *Kinematic Methods in High-energy Physics*. SSRSS Series. Harwood Academic Publishers, 1989.

[14] O. Klein and T. Nishina. Über die Streuung von Strahlung durch freie Elektronen nach der neuen relativistischen Quantendynamik von Dirac. *Zeitschrift für Physik*, 52(11-12):853–868, 11 1929.

[15] J.D. Jackson. *Classical Electrodynamics*. Wiley, 1998.

[16] G.B Rybicki and A.P Lightman. *Radiative processes in astrophysics*. John Wiley & Sons, 1979.

[17] F. Schwabl. *Advanced quantum mechanics (fourth edition)*. Springer Berlin Heidelberg, 2008.

[18] ATLAS Collaboration. The Athena codebase. 2021. https://doi.org/10.5281/zenodo.4772550.

[19] G. Barrand et al. Gaudi — a software architecture and framework for building hep data processing applications. *Computer Physics Communications*, 140(1):45–55, 2001. CHEP2000.

[20] G. Corti and M. Cattaneo et al. Software for the LHCb experiment. *IEEE Transactions on Nuclear Science*, 53(3):1323–1328, 6 2006.

[21] ATLAS Collaboration. The ATLAS Simulation Infrastructure. *Eur.Phys.J.C*, 70(3):823–874, 1 2010.

[22] E. Ritsch. Concepts and Plans towards fast large scale Monte Carlo production for the ATLAS Experiment. *J. Phys. Conf. Ser.*, 523:012035, 2014.

[23] C. Debenedetti. Concepts for fast large scale Monte Carlo production for the ATLAS experiment. *J. Phys. Conf. Ser.*, 513:022006, 2014.

[24] GEANT4 Collaboration. Geant4 developments and applications. *IEEE Trans.Nucl.Sci.*, 53(1):270, 2 2006.

[25] Freytsis M. et al. Coleman, E. Simulation strategies using FATRAS and Geant4 for a future upgrade of the ATLAS tracking detectors. *Journal of Physics: Conference Series*, 219(3):032021, 4 2010.

[26] H. Messel and D. F. Crawford. Electron–photon shower distribution function; tables for lead, copper, and air absorbers. page 1512, 1970.

[27] Geant4 Collaboration. Compton scattering — Physics Reference Manual 11.3 documentation. volume Rev 9.0:. 2024.

[28] J. C. Butcher and H. Messel. Electron number distribution in electron-photon showers in air and aluminium absorbers. *Nuclear Physics*, 20(C):15–128, 10 1960.